

Determination of Spin–Orbit Branching Fractions in the Photodissociation of Halogenated Hydrocarbons[†]

H. Fan and S. T. Pratt*

Argonne National Laboratory, Argonne, Illinois 60439

Received: October 25, 2006

Two methods based on vacuum ultraviolet (vuv) photoionization are presented for the determination of the spin–orbit branching fractions of the halogen atom produced in the photodissociation of halogenated hydrocarbons. Both methods make use of differences in the photoionization cross sections of the $^2P_{3/2}$ ground state and the $^2P_{1/2}$ excited-state of the neutral halogen atom. In the first approach, measurements of the total photoionization signal of the halogen atom are made at several vuv wavelengths, and the difference in the wavelength dependences for the $^2P_{3/2}$ and $^2P_{1/2}$ atoms allows the extraction of the branching fractions. In the second approach, the vuv wavelength is set close to the ionization threshold of the $^2P_{3/2}$ atom (well above that of the $^2P_{1/2}$ atom), and measurements are made at several electric field strengths, which shift the ionization threshold and thus vary the photoionization cross sections. In both methods, the relative cross sections of the ground- and excited-state atoms are determined by using the known branching fractions for the 266 nm photodissociation of methyl iodide. These methods are applied to the photodissociation of isopropyl iodide and allyl iodide, two systems for which standard ion-imaging techniques do not provide unique branching fractions.

I. Introduction

Historically, halogenated hydrocarbons have played an important role as prototypical systems for the study of photodissociation dynamics.^{1–4} While many aspects of these systems have been investigated in substantial detail, one of the best studied observables has been the branching ratio between the two spin–orbit components of the ground state configuration of the halogen atom fragment following photoexcitation in the near-ultraviolet. In an early discussion of the near-ultraviolet absorption spectrum of the alkyl halides, Mulliken^{5,6} showed that there were three optically allowed states based on excitation from the lone pair p orbital of the halogen to the lowest energy ns σ^* orbital, and he labeled these 3Q_0 , 1Q_1 , and 3Q_1 . For the mono-halogenated R–X molecule (where R is the hydrocarbon and X is the halogen), Mulliken^{5,6} showed that the 3Q_1 and 1Q_1 states are diabatically correlated with the R + X $^2P_{3/2}$ limit, and the 3Q_0 state is correlated with the R + X $^2P_{1/2}$ limit. However, interactions among these surfaces lead to the mixing of their characters and transitions between them. Thus, both the relative excitation probabilities to the different surfaces and the interactions among them play an important role in determining the spin–orbit branching ratio at a given wavelength. When R is an unsaturated radical, excitation from the lone pair σ orbital or from the π system into the corresponding π^* orbital(s) can overlap the transition to the σ^* orbital, leading to more complex behavior.^{7,8} Nevertheless, the spin–orbit branching fraction in the R + X dissociation channel still provides important information on the dissociation process.

Many different approaches have been developed to determine spin–orbit branching ratios in R–X molecules.² Given the rapidly increasing popularity of ion-imaging techniques,^{9,10} the present discussion focuses on spin–orbit branching ratio

measurements that employ ionization-based detection. Intensity measurements of the ion signal following resonant multiphoton ionization of the $^2P_{3/2}$ and $^2P_{1/2}$ halogen atoms can be used to determine the spin–orbit branching ratio if the relative line strengths of the two ionization processes can be determined.^{11–13} For Cl, Br, I, and many other atoms, the most suitable such process corresponds to two-photon resonant, three-photon ionization [(2 + 1) ionization]. If, as in the case of Cl atoms, the resonant intermediate levels of the ionization schemes for the $^2P_{3/2}$ and $^2P_{1/2}$ levels belong to the same multiplet,¹⁴ and if the transition wavelengths are close to each other, it can be sufficient to use theoretical two-photon line strengths to compare the signals from the two processes. However, because the detection process is nonlinear and thus very sensitive to the laser intensity, it is best to have an internal calibration of the relative line strengths.^{11,13} Such a calibration is generally also necessary for the detection of Br and I, because the spin–orbit splitting is so large that either the detection wavelengths will differ substantially or the intermediate levels in the ionization scheme will belong to different multiplets, and thus be difficult to compare.

A second ionization-based approach to determining spin–orbit branching ratios can be used in conjunction with translational spectroscopy or ion-imaging if the two spin–orbit states are resolved in the translational energy distribution, or $P(E_T)$ curve (where E_T is the total translational energy). If the ionization cross section is independent of the spin–orbit state of the atom, or if the relative photoionization cross sections of the $^2P_{3/2}$ and $^2P_{1/2}$ states are known, and if the angular distributions of the fragments are taken into account, the different components of the $P(E_T)$ curve determined from the X⁺ signal can be integrated to provide the branching ratio. Alternatively, if the ionization cross section of the R fragment is independent of internal energy, the $P(E_T)$ curve determined from the R⁺ signal can be used to determine the branching ratio

[†] Part of the special issue “James A. Miller Festschrift”.

in the same manner.¹⁵ Unfortunately, in many examples of interest, the $P(E_T)$ curves for the $^2P_{3/2}$ and $^2P_{1/2}$ components are strongly overlapped.^{15,16} For example, although the two spin-orbit components for the 266 nm photodissociation of methyl iodide, ethyl iodide, and *n*-propyl iodide in the classic paper of Riley and Wilson are well-resolved,¹ they are completely overlapped for isopropyl iodide. This observation is confirmed in more recent experiments in which separate $^2P_{3/2}$ and $^2P_{1/2}$ distribution were recorded by using $(2 + 1)$ ionization of the iodine atoms.¹⁵

Clearly it would be useful to have an ionization-based method to determine spin-orbit branching ratios that is straightforward to calibrate and is also applicable when the corresponding $P(E_T)$ distributions are not well-resolved. In this paper, we address this desire with two different approaches, both of which are based on monitoring the total X^+ ion signal following the vuv photoionization of the halogen atom. For experimental simplicity, the halogen atom is iodine in all of the examples discussed here but, in principle, the methods are quite general.

The first approach makes use of the different wavelength dependences of the photoionization cross sections for the $^2P_{3/2}$ and $^2P_{1/2}$ atoms,¹⁷ as well as the ability to calibrate these relative cross sections using the photodissociation of CH_3I at 266 nm.^{18,19} This photodissociation process is particularly useful because the $^2P_{3/2}$ and $^2P_{1/2}$ components of the $P(E_T)$ distribution are well-resolved¹ and because the spin-orbit branching ratio has been determined previously in numerous different measurements.^{18,19} The basic idea of this approach is to photodissociate CH_3I at 266 nm and record I^+ images at a series of photoionization wavelengths. Because the spin-orbit branching ratio is known for the photodissociation of CH_3I at 266 nm,¹⁸ it can be used along with the integrated intensities of the $^2P_{3/2}$ and $^2P_{1/2}$ components of the $P(E_T)$ curve determined from the image to extract the relative photoionization cross sections for the two components at a given photoionization energy. The series of photoionization wavelengths is chosen such that the relative photoionization cross sections vary substantially. In the present experiments, this is achieved by tuning the photoionization energy through the ionization threshold of the $^2P_{3/2}$ atoms, which is well above the ionization threshold of the $^2P_{1/2}$ atoms.^{17,20} By tuning through the ionization threshold, it is straightforward to find energies at which the ratio of the $^2P_{3/2}$ to $^2P_{1/2}$ cross sections varies from zero to approximately 20. Once these energies and relative cross sections are known, they can be used to determine the spin-orbit branching ratios for other photo-dissociation processes that produces $\text{I } ^2P_{3/2}$ and $^2P_{1/2}$ simply by recording the total I^+ ionization signal at each energy and solving the resulting set of equations. The details of this approach are discussed in section III.A., following the description of the experimental details in section II.

One difficulty with this first approach is that if the wavelength of the vuv light is varied substantially, it becomes necessary to monitor the pulse energy accurately. In addition, when sharp resonances are present in the photoionization cross section of either spin-orbit state, the wavelengths must be accurately reproduced. The second approach to determining spin-orbit branching ratios is aimed at addressing these potential difficulties. As in the first approach, the method is calibrated by using the photodissociation of CH_3I at 266 nm. However, in this approach the photoionization energy is fixed just below the ionization threshold of the iodine $^2P_{3/2}$ ground state. Images are then recorded as a function of the DC electric field in the interaction region. Although this field is part of the lensing field for velocity map ion imaging,²¹ it can be tuned over a relatively

small range without significantly affecting the image resolution. This DC field also shifts the effective ionization potential of the $^2P_{3/2}$ atoms, which can then be tuned through the photon energy.²² Thus, the photoionization cross section of the $^2P_{3/2}$ atoms can be varied substantially, with no significant effect on the photoionization cross section of the $^2P_{1/2}$ atoms. The I^+ images recorded at a series of electric fields can be used with the true branching ratio to determine the relative photoionization cross sections at the chosen wavelength as a function of electric field. As in the first approach, these cross sections can be used to determine the spin-orbit branching ratios for other photo-dissociation processes that produces $\text{I } ^2P_{3/2}$ and $^2P_{1/2}$ simply by recording the total I^+ ionization signal at each field strength and solving the resulting set of equations. The advantages of this approach are that the photoionization energy does not need to be tuned, and that the precise wavelength need not be known so long as it is stable. The details of this approach are described in section III.B, and the applications of the two approaches to isopropyl iodide and allyl iodide are described in section III.C. A summary and conclusions are presented in section IV.

II. Experiment

The apparatus and laser systems have been described in detail previously.^{21,23} The apparatus consists of a pulsed, skimmed molecular beam source coupled to a colinear time-of-flight/velocity-map imaging spectrometer. The room-temperature sample was prepared by seeding $\sim 2\%$ of the appropriate alkyl iodide in He with a total stagnation pressure of ~ 1500 Torr. The skimmed molecular beam was crossed in the interaction region at a 90° angle by both the photodissociation and photoionization beams. The photodissociation beam was provided by either the 266 nm fourth harmonic of a Nd:YAG laser or by the 193 nm light from an ArF excimer laser. The dissociation beam was reduced in size by an aperture, and the polarization was purified by using a Glan-laser polarizer. The resulting beam was linearly polarized parallel to the face of the detector, and was loosely focused into the interaction region.

In the present experiments, the vacuum ultraviolet (vuv) photoionization beam was generated by using two-photon resonant, difference frequency mixing in Kr (i.e., $\omega_{\text{vuv}} = 2\omega_1 - \omega_2$). The light for the two-photon transition, ω_1 , at 202.315 nm (corresponding to the Kr $5p'1/2_0 \leftarrow ^1S_0$ transition²⁴) was generated by mixing the frequency-doubled output of a Nd:YAG-pumped dye laser with the corresponding dye fundamental by using a BBO crystal. The tunable beam, ω_2 , was generated by using a second Nd:YAG-pumped dye laser. The two beams were combined by using a dichroic mirror and focused into a gas cell containing ~ 30 – 300 Torr of Kr. The diverging ω_1 , ω_2 , and vuv beams were refocused into the interaction region by using a LiF lens that also served as the window into the apparatus. This lens was aligned slightly off-center so that only the vuv beam interacted with the sample. The polarizations of all three beams were parallel to the face of the detector and to that of the dissociation beam. The wavelengths of ω_1 and ω_2 were determined by measuring the fundamentals by using a commercial wavemeter. The relative intensities were controlled by using neutral density filters in the photodissociation beam or in ω_1 or ω_2 . For the present iodine images, all of the signal came from the two-color process, as no signal was observed when only the photodissociation or photoionization beams were present.

The pulse durations of both the photodissociation and photoionization beams were approximately 10 ns, and the former was arranged to arrive in the interaction region approximately

30 ns ahead of the latter. The timing of the pulsed molecular beam was adjusted to minimize the contribution of clusters to the signal. For the mass spectra, the detector voltages were fixed to allow recording of the full range of flight times, while for images the detector was gated on the time-of-flight for the species of interest. Mass spectra were recorded by using a digital oscilloscope and averaging for 300 laser shots, while a typical image was recorded by averaging for 10 000 laser shots. The latter data were available in both raw and centroided form. The images were reconstructed by using the BASEX program described by Dribinski et al.,²⁵ yielding the three-dimensional velocity distributions and photofragment angular distribution parameters. The images were calibrated by comparison with images of propargyl chloride dissociation that have been discussed previously,²⁶ and with images produced by the 193 nm photodissociation of methyl iodide.²⁷

III. Results and Discussion

A. Spin–Orbit Branching Ratios by Wavelength-Dependent Photoionizations. The ground state of I^+ corresponds to the $...5s^25p^4$ configuration and a 3P_2 electronic state.²⁰ The near-threshold photoionization spectrum of $I\ ^2P_{3/2}$ has been reported previously by Berkowitz et al.,¹⁷ and it shows substantial autoionization structure in the form of both broad and sharp resonances converging to the excited 3P_1 , 3P_0 , 1D_2 , and 1S_0 levels of the ion, all of which belong to the same configuration as the ground state. The $\Delta J = 0, \pm 1$ dipole selection rule for single-photon excitation implies that all of these resonances have $J' = 1/2, 3/2, \text{ or } 5/2$. The corresponding photoionization spectrum of $I\ ^2P_{1/2}$ has not been reported, but the positions (if not the intensities or line shapes) of the expected resonances can be readily calculated by subtracting the $^2P_{1/2}$ spin–orbit energy of 7603.149 cm^{-1} from the transition energy in the $^2P_{3/2}$ spectrum,¹⁷ and restricting the angular momentum of the upper state to $1/2$ or $3/2$.

The spin–orbit branching ratio measurements using the wavelength dependence of the relative photoionization cross sections for $I\ ^2P_{3/2}$ and $^2P_{1/2}$ are performed as follows. First, the relative photoionization cross sections for the two spin–orbit states must be determined at a series of photoionization energies. The spin–orbit branching ratio for the photodissociation of CH_3I at 266 nm is well-known, and is used for calibration. Iodine ion images are recorded for this process at the desired photoionization energies. The reconstructed images provide the translational energy distribution, or $P(E_T)$ curve, in which the $I\ ^2P_{3/2}$ and $^2P_{1/2}$ components are well resolved. [See, for example, Figure 4 of ref 29.] The integrated intensities of each component is proportional to the product of the branching fraction and the relative photoionization cross section for that spin–orbit state at that photoionization energy. In other words:

$$\frac{I_{(^2P_{3/2})}(h\nu)}{I_{(^2P_{1/2})}(h\nu)} = \frac{B_{(^2P_{3/2})}\sigma_{(^2P_{3/2})}(h\nu)}{B_{(^2P_{1/2})}\sigma_{(^2P_{1/2})}(h\nu)} \quad (1)$$

The $I_{(^2P_j)}(h\nu)$ are the experimentally determined integrated intensities of the two spin–orbit components in the $P(E_T)$ distributions derived from the images. The $B_{(^2P_j)}$ are the branching fractions for the two spin–orbit states, and $B_{(^2P_{3/2})}/B_{(^2P_{1/2})}$ is the branching ratio. The $\sigma_{(^2P_j)}(h\nu)/\sigma_{I_{(^2P_{1/2})}}(h\nu)$ are the unknown relative photoionization cross sections for the two components, and the ratio $\sigma_{(^2P_{3/2})}(h\nu)/\sigma_{(^2P_{1/2})}(h\nu)$ can be extracted from eq 1.

In the present experiments, the photoionization energies are chosen just below and above the $^2P_{3/2}$ ionization threshold, and

thus the $\sigma_{(^2P_{3/2})}(h\nu)$ value changes dramatically in this energy region.¹⁷ As discussed in more detail below, the DC electric field in the interaction region shifts the effective ionization threshold by²²

$$\Delta(\text{cm}^{-1}) = 6.1\sqrt{F(\text{V/cm})} \quad (2)$$

where Δ is the shift and F is the electric field, with the result that photoionization energies between 84190 and 84200 cm^{-1} were used. [The adiabatic ionization energy of $I\ ^2P_{3/2}$ is $84295.1 \pm 0.2\text{ cm}^{-1}$.²⁹ The $I\ ^2P_{3/2}$ photoionization spectrum in the region lying 7603.149 cm^{-1} above this threshold is free of sharp resonances, and shows only a slow decrease in cross section with increasing photon energy as a result of the Beutler-Fano profile of an extremely broad d resonance.¹⁷ Because the range of photoionization energies used here is so small, for the present study $\sigma_{(^2P_{1/2})}(h\nu)$ is assumed to be independent of photoionization energy. With this assumption, the measurement of the relative intensities of the two spin–orbit states as a function of wavelength provides the wavelength dependence of $\sigma_{(^2P_{3/2})}(h\nu)$.

With a knowledge of the wavelength dependence of the relative photoionization cross sections $\sigma_{(^2P_{3/2})}(h\nu)$ and $\sigma_{(^2P_{1/2})}(h\nu)$, the total I^+ signal as a function of wavelength, $I_+(h\nu)$, can be used to determine the spin–orbit branching ratio for any dissociation process producing the I fragment. In particular,

$$I_+(h\nu) = A[B_{(^2P_{1/2})}\sigma_{(^2P_{1/2})}(h\nu) + B_{(^2P_{3/2})}\sigma_{(^2P_{3/2})}(h\nu)] \quad (3)$$

where A is an proportionality constant. Using (1) the $\sigma_{(^2P_j)}(h\nu)$ determined from the images, (2) the $I_+(h\nu)$ measured in the mass spectrum, (3) the observation that the $B_{(^2P_{3/2})}$ values are independent of $h\nu$, and (4) the identity $B_{(^2P_{3/2})} = 1 - B_{(^2P_{1/2})}$, measurements at two values of $h\nu$ lead to a set of two equations that can be solved for the proportionality constant and the two branching fractions. Alternatively, measurements at additional values of $h\nu$ lead to an over-determined set of equations that can be used to extract best fit values of the branching fractions. This approach can be validated by performing the I^+ intensities measurements on the 266 nm photodissociation of CH_3I , which provides a useful consistency check as discussed in section III.C below.

Figure 1 shows the $P(E_T)$ curves generated for the 266 nm photodissociation of CH_3I from the I^+ images recorded at a series of photoionization energies. Although the $^2P_{1/2}$ component is present at each energy, the $^2P_{3/2}$ component only grows in as the photon energy passes through the field-shifted $^2P_{3/2}$ ionization threshold. It is clear even from visual inspection of Figure 1 that, as indicated by the relative areas of the two components, the cross section ratio $\sigma_{(^2P_{3/2})}(h\nu)/\sigma_{(^2P_{1/2})}(h\nu)$ varies substantially over this very small range ($\sim 5.3\text{ cm}^{-1}$) of vuv photon energies. The actual cross section ratios determined from Figure 1 are given in Table 1. Figure 2 shows a scan of the total I^+ ion signal as a function of the vuv photon energy following the photodissociation of CH_3I at 266 nm. Below approximately 84194 cm^{-1} , the signal comes solely from ionization of the $^2P_{1/2}$ atoms, while the sharp rise above this energy corresponds to the onset of ionization of the $^2P_{3/2}$ atoms. The photoionization spectrum of Berkowitz et al.¹⁷ shows a sharp autoionization resonance just above threshold, so the rise in signal observed in Figure 2 may result from a combination of direct photoionization and autoionization. [Technically, the latter is forced autoionization,²² as the photon energy is still below the adiabatic ionization threshold and autoionization is only allowed into the field shifted continuum.] Because the ionization onset of the $^2P_{3/2}$ components is so sharp, the cross section ratios in Table 1 are very sensitive

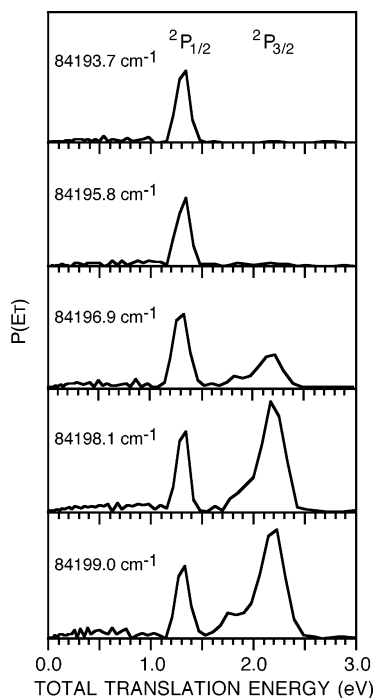


Figure 1. The $P(E_T)$ curves generated from the I^+ images recorded following the 266 nm photodissociation of CH_3I . The vuv photon energies are given in each frame and the baseline of the y-axis corresponds to zero signal.

to the precise vuv energy at this threshold. As a result, in practice the total ionization measurements for the branching fraction determinations are only made at two wavelengths clearly above and below this sharp onset.

B. Spin—Orbit Branching Ratios by Electric-Field-Dependent Photoionization. The shift of the effective ionization threshold as a function of the electric field in the interaction region provides a second approach to varying the relative photoionization cross sections of the $^2P_{3/2}$ and $^2P_{1/2}$ states near the $^2P_{3/2}$ ionization threshold. In particular, if the vuv photon energy is fixed close to the ionization threshold of Figure 2 and the electric field is scanned, the effective ionization energy can be scanned through the photon energy. Such scans are shown in Figure 3 for the I^+ signal produced following the 266 nm photodissociation of both CH_3I and $i-C_3H_7I$ at 266 nm, with the photoionization energy was fixed at 84198.5 cm^{-1} . The x-axis of the plot corresponds to the electric field in the interaction region. Note that in both spectra I atoms are being ionized and detected, and it is only the ratio of $^2P_{1/2}$ to $^2P_{3/2}$ atoms that changes as a result of the different samples. For the lowest field strengths in Figure 3, the ionization signal is only produced by photoionization of the $^2P_{1/2}$ atoms, while at the highest field, the $^2P_{3/2}$ atoms are also ionized. The signal levels below and above this threshold are relatively constant. Because the signal for $i-C_3H_7I$ is below the signal for CH_3I below the threshold and above the signal for CH_3I above the threshold, it is already clear that the $^2P_{1/2}$ branching fraction for $i-C_3H_7I$ is smaller than that for CH_3I .

Measurements of the relative photoionization cross sections as a function of the electric field are performed by recording images following the 266 nm photodissociation of CH_3I at a fixed photoionization energy but as a function of the electric field in the interaction region. Figure 4 shows a series $P(E_T)$ curves extracted from the reconstructed images recorded as a function of electric field at a photoionization energy of 84198.5 cm^{-1} . The electric field was varied by changing the potential

of only one of the plates defining the interaction region. As a result, the resolution of the $P(E_T)$ distributions changes somewhat for the different voltages. Nevertheless, the resolution in all of the distributions is sufficient to resolve the two spin—orbital components, and thus allows the extraction of the relative cross section ratio as a function of the field. The cross section for the $^2P_{3/2}$ state clearly undergoes a sharp rise at the critical electric field. In contrast, because there are no resonances near the energy corresponding to excitation of the $^2P_{1/2}$ level,¹⁷ the electric field is expected to have a negligible effect on the cross section for the $^2P_{1/2}$ level. It is assumed in what follows that the $^2P_{1/2}$ cross section is independent of the field strength.

Because the interaction region is actually within an electrostatic immersion lens,²¹ the electric field is not expected to be uniform. In spite of this, the sharp step in Figure 3 is observed very close to the electric field expected based on eq 2 and the adiabatic ionization potential of I $^2P_{3/2}$, and the step is at the same position for both samples. This suggests that the ionization occurs in a relatively small volume with a reasonably well-defined electric field. In principle, the position of the threshold in Figure 3 could be sensitive to the position of the laser interaction region. Given that the signal requires the overlap of the two beams, however, it is likely that significant displacement of one of the beams will result in the disappearance of the signal, rather than a shift of the effective threshold. Nevertheless, for this reason, and because the threshold is quite sharp, the I^+ intensities for the branching ratio measurements were made at just two electric fields corresponding to well below and well above the $^2P_{3/2}$ threshold.

Given the field dependence of the relative photoionization cross sections, eq 1 can be modified to give the following:

$$\frac{I_{(^2P_{3/2})}(F)}{I_{(^2P_{1/2})}(F)} = \frac{B_{(^2P_{3/2})}\sigma_{(^2P_{3/2})}(F)}{B_{(^2P_{1/2})}\sigma_{(^2P_{1/2})}(F)} \quad (1a)$$

where now the ion intensities and photoionization cross sections are a function of the field, rather than the photoionization energy. Similarly, eq 3 is modified to

$$I_{I^+}(F) = A[B_{(^2P_{1/2})}\sigma_{(^2P_{1/2})}(F) + B_{(^2P_{3/2})}\sigma_{(^2P_{3/2})}(F)] \quad (3a)$$

Functionally, these equations are used in the same manner as in the energy-dependent experiments, and once the $\sigma_{(^2P_{3/2})}(F)$ and $\sigma_{(^2P_{1/2})}(F)$ are determined, measurements of the total I^+ intensity as a function of electric field then allow the extraction of the branching fractions.

C. Spin—Orbit Branching Ratios for Isopropyl Iodide and Allyl Iodide. As described above, the experiments were performed in two parts. First, the relative photoionization cross sections for the $^2P_{3/2}$ and $^2P_{1/2}$ levels were determined as a function of vuv wavelength or electric field by recording a series of images of I following the 266 nm photodissociation of CH_3I . These relative cross sections were corrected by using the previously determined $^2P_{1/2}$ branching fraction for this process¹⁸ of 0.76. Second, the total ion signal was determined at the wavelengths or electric fields of the cross section measurements. Both the wavelength and field dependences show plateaus above and below the ionization threshold for the $^2P_{3/2}$ level, and all of the intensity measurements used here were performed in these plateau regions. As seen in Table 1, when multiple measurements of the relative cross sections were performed, there is some scatter in the values, but they are in generally good agreement.

TABLE 1: Relative Photoionization Cross Sections and I $^2P_{1/2}$ Branching Fractions^a

| molecule (dissociation $h\nu$) | ionization ($h\nu$ in cm^{-1}) | $\sigma(^2P_{3/2})(h\nu)/\sigma(^2P_{1/2})(h\nu)$ | F (V/cm) | $\sigma(^2P_{3/2})(F)/\sigma(^2P_{1/2})(F)$ | $B(^2P_{1/2})$ |
|---|--|---|---------------|---|-----------------|
| CH ₃ I (266 nm) | 84189.9 | 0.0 | | | 0.83 ± 0.10 |
| | 84199.5 | 8.57 | 214.0 | 0.0 | 0.81 ± 0.10 |
| | 84198.5 ^b | | 247.3 | 9.50 | |
| | | | 207.3 | 0.0 | 0.76 ± 0.10 |
| | | | 250.7 | 9.12 | |
| | | | 207.3 | 0.0 | 0.80 ± 0.10 |
| <i>i</i> -C ₃ H ₇ I (266 nm) | 84189.9 | 0.0 | | | 0.57 ± 0.10 |
| | 84199.5 | 8.57 | 214.0 | 0.0 | 0.53 ± 0.10 |
| | 84198.5 | | 247.3 | 9.50 | |
| | | | 207.3 | 0.0 | 0.90 ± 0.10 |
| | | | 250.7 | 9.12 | |
| | | | 207.3 | 0.0 | 0.61 ± 0.10 |
| C ₃ H ₅ I (266 nm) | 84198.5 | | 214.0 | 0.0 | |
| | | | 254.0 | 8.84 | |
| C ₃ H ₅ I (193 nm) | 84198.5 | | 214.0 | 0.0 | |
| | | | 254.0 | 8.84 | |

^a Additional measurements were performed at several different wavelengths above the $^2P_{3/2}$ threshold for the first method and at several different electric field strengths for the second method. These results are similar to the tabulated values and are reflected in the error bars. ^b These data represent the results of relative cross section measurements (i.e., imaging data) on three separate days, and they provide an indication of the reproducibility of the approach.

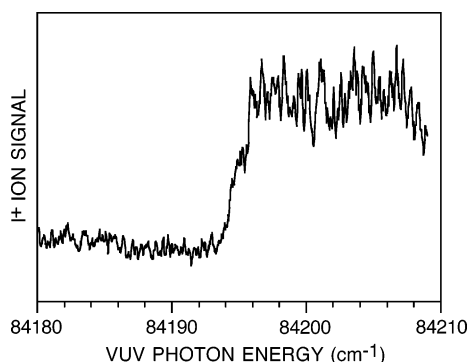


Figure 2. Scan of the total I⁺ ion signal as a function of the vuv photon energy following the photodissociation of CH₃I at 266 nm. Although the adiabatic ionization energy of I $^2P_{3/2}$ is $84295.1 \pm 0.2 \text{ cm}^{-1}$, the electric field in the interaction region shifts the effective ionization energy into the range of the figure.

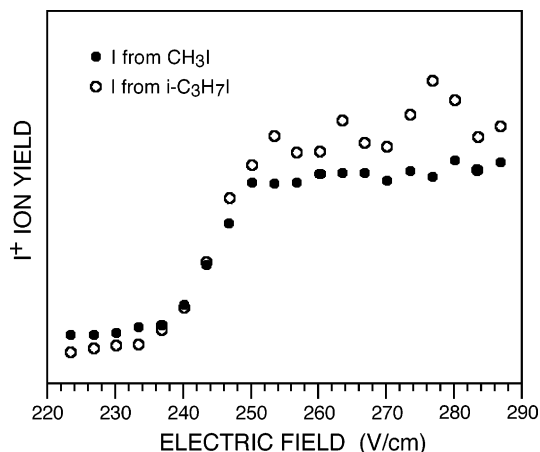


Figure 3. I⁺ signal produced following the 266 nm photodissociation of CH₃I and *i*-C₃H₇I at 266 nm, with the vuv photon energy fixed at 84198.5 cm^{-1} . The electric field in the interaction region was scanned by varying the voltage across the two plates that define the interaction region. The two plates are separated by 1.5 cm. The CH₃I data are shown as solid circles and the *i*-C₃H₇I data are shown as open circles.

As a test of the two approaches, intensity measurements were performed on the I $^2P_{3/2}$ and $^2P_{1/2}$ from CH₃I at 266 nm, and the relative cross sections determined from the images were used to determine the branching fractions. Table 1 shows that

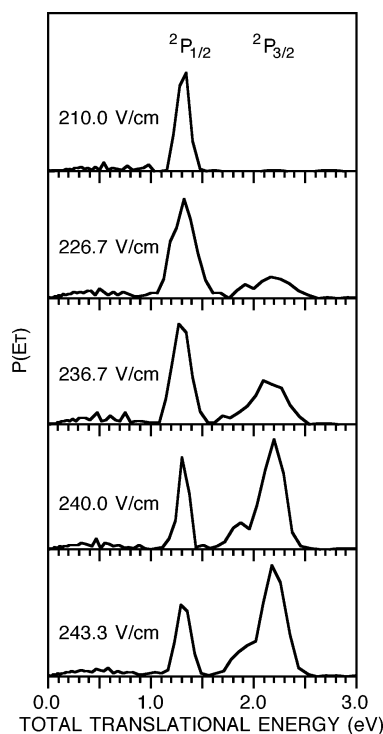


Figure 4. $P(E_T)$ curves generated from the I⁺ images recorded following the 266 nm photodissociation of CH₃I and with a photoionization energy of 84198.5 cm^{-1} . The voltage across the interaction region is indicated in each frame.

both the wavelength-dependent and field-dependent measurements yield branching fractions slightly higher, but in good agreement with the known values¹⁸ for CH₃I. These measurements thus provide some confidence in the two methods and allow us to estimate an uncertainty in the branching fractions of approximately ± 0.10 . Intensity measurements were then performed on the other samples. In particular, Table 1 also shows the branching fractions determined for the photodissociation for *i*-C₃H₇I at 266 nm, and for the photodissociation of allyl iodide, C₃H₅I, at both 266 and 193 nm. Uma and Das³⁰ have previously used two-photon laser-induced fluorescence to determine the $^2P_{1/2}$ branching fraction for the 266 nm photodissociation of *i*-C₃H₇I, and reported a value of $B(^2P_{1/2}) = 0.44$

± 0.03 . This value is slightly lower than the values in Table 1, but the values agree within their error bars.

To our knowledge, there are no previous measurements of the $I^2P_{3/2}$ and $^2P_{1/2}$ branching fractions for allyl iodide at either 266 or 193 nm. Allyl iodide absorbs only weakly at 266 nm, and the absorption is likely to the σ^* orbital, resulting in direct, fast dissociation. The value of the branching fraction $B(^2P_{1/2}) = 0.92 \pm 0.10$ suggests that at this wavelength, excitation to the 3Q_0 state dominates and that the interaction with the 3Q_1 and 1Q_1 states is minor. At 193 nm, both the σ^* and π systems will be excited and the dissociation dynamics are expected to be more complicated. The value of the branching fraction $B(^2P_{1/2}) = 0.60 \pm 0.10$ reflects this situation, and is consistent with our recent analysis¹⁸ of imaging experiments on the photodissociation of allyl iodide at 193 nm, which suggested that the $B(^2P_{1/2})$ value was somewhat larger than previously suspected.³¹ In those experiments,¹⁸ it was not possible to extract the branching fractions by fitting the $P(E_T)$ curves because the distributions for the $^2P_{3/2}$ and $^2P_{1/2}$ states were too similar to each other to yield a unique fit to the total distribution. This example thus provides a demonstration of the practical utility of the two approaches discussed here.

IV. Conclusion

Two approaches to determine spin-orbit branching fractions in photodissociation experiments on halogen-containing molecules have been discussed. Both methods employ a combination of vuv photoionization and ion imaging, and both circumvent difficulties associated with overlapping $P(E_T)$ distributions for the two spin-orbit states of the halogen molecule. The simpler approach is that based on a fixed photoionization photon energy and shifting the ionization threshold by varying the electric field in the ionization region. The methods have been validated by using the photodissociation of CH_3I , and give good agreement with other methods for the $^2P_{3/2}$ and $^2P_{1/2}$ branching fractions in *i*- $\text{C}_3\text{H}_7\text{I}$. The electric field method has also been used to determine the spin-orbit branching fractions for allyl iodide, which had not been determined previously.

The methods described here should be generalizable to the determination of spin-orbit branching fractions for other halogens or other atoms. The only requirement is that the different spin-orbit components can be resolved in the ion images for the photodissociation of at least one precursor molecule, and that the branching fractions for this precursor can be accurately determined either through a combination of imaging techniques or by other approaches. Once the details of the calibration molecule are established, this molecule can be used to determine the energy or electric-field dependence of the relevant photoionization cross sections. In some instances, it may not always be desirable, or even possible, to work at photoionization energies close to the adiabatic ionization energy. In addition, when three or more spin-orbit states can be

populated, further information will be necessary. In this case it is likely that the approach based on the energy dependence of the cross section will be more favorable. In particular, it should be possible to choose energies corresponding to the excitation of autoionizing resonances to maximize, in turn, the relative cross sections of each of the spin-orbit states of interest.

Acknowledgment. This work was supported by the U.S. Department of Energy, Office of Science, Office of Basic Energy Sciences, Division of Chemical Sciences, Geosciences, and Biological Sciences under Contract No. DE-AC02-06CH11357.

References and Notes

- (1) Riley, S. J.; Wilson, K. R. *Disc. Faraday Soc.* **1972**, *53*, 132.
- (2) Leone, S. R. *Adv. Chem. Phys.* **1982**, *50*, 255.
- (3) Ashfold, M. N. R.; Baggott, J. E. Eds. *Molecular Photodissociation Dynamics*; Royal Society of Chemistry: London, 1987.
- (4) Schinke, R. *Photodissociation Dynamics*; Cambridge University: Cambridge, U.K., 1993.
- (5) Mulliken, R. S. *J. Chem. Phys.* **1940**, *8*, 382.
- (6) Mulliken, R. S. *Phys. Rev.* **1942**, *61*, 277.
- (7) Robin, M. B. *Higher Excited States of Polyatomic Molecules*; Academic: New York, 1975; Vols I–II.
- (8) Robin, M. B. *Higher Excited States of Polyatomic Molecules*; Academic: New York, 1985; Vol. III.
- (9) Suits, A. G.; Continetti, R. E. *Imaging in Chemical Dynamics*; American Chemical Society: Washington, DC, 2001.
- (10) Chandler, D. W.; Parker, D. H. *Adv. Photochem.* **1999**, *25*, 59.
- (11) Park, M. S.; Lee, K. W.; Jung, K.-H. *J. Chem. Phys.* **2001**, *114*, 10368.
- (12) Liu, Y.; Butler, L. J. *J. Chem. Phys.* **2004**, *121*, 11016.
- (13) Liu, Y.; Lau, K. C.; Butler, L. J. *J. Phys. Chem. A* **2006**, *110*, 5379.
- (14) Moore, C. E. *Atomic Energy Levels*; Nat. Stand. Ref. Data Ser., Nat. Bur. Stand. 35; Dept. of Commerce: Washington, DC, 1971; Vol. I.
- (15) Fan, H.; Pratt, S. T. *J. Chem. Phys.* **2005**, *123*, 204301.
- (16) Fan, H.; Pratt, S. T. *J. Chem. Phys.* **2006**, *125*, 144302.
- (17) Berkowitz, J.; Batson, C. H.; Goodman, G. L. *Phys. Rev. A* **1981**, *24*, 149.
- (18) See, for example: Eppink, A. T. J. B.; Parker, D. H. *J. Chem. Phys.* **1998**, *109*, 4758 and references therein.
- (19) Eppink, A. T. J. B.; Parker, D. H. *J. Chem. Phys.* **1999**, *110*, 832.
- (20) Moore, C. E. *Atomic Energy Levels*; Nat. Bur. Stand. Circular 467; Dept. of Commerce: Washington, DC, 1957; Vol. III.
- (21) Eppink, A. T. J. B.; Parker, D. H. *Rev. Sci. Instrum.* **1997**, *68*, 3477.
- (22) Gallagher, T. F. *Rydberg Atoms*; Cambridge University: New York, 1994.
- (23) Aguirre, F.; Pratt, S. T. *J. Chem. Phys.* **2003**, *118*, 1175.
- (24) Moore, C. E. *Atomic Energy Levels*; Nat. Bur. Stand. Circular 467; Dept. of Commerce: Washington, DC, 1952; Vol. II.
- (25) Dribinski, V.; Ossadtchi, A.; Mandelshtam, V.; Reisler, H. *Rev. Sci. Instrum.* **2002**, *73*, 2634.
- (26) McCunn, L. R.; Bennett, D. I. G.; Butler, L. J.; Fan, H.; Aguirre, F.; Pratt, S. T. *J. Phys. Chem. A* **2006**, *110*, 843.
- (27) Continetti, R. E.; Balko, B. A.; Lee, Y. T. *J. Chem. Phys.* **1988**, *89*, 3383.
- (28) Aguirre, F.; Pratt, S. T. *J. Chem. Phys.* **2005**, *122*, 234303.
- (29) Minnhagen, L. *Ark. Fys.* **1962**, *21*, 415.
- (30) Uma, S.; Das, P. K. *J. Chem. Phys.* **1996**, *104*, 4471.
- (31) Szpunar, D. E.; Morton, M. L.; Butler, L. J.; Regan, P. M. *J. Phys. Chem. B* **2002**, *106*, 8086.